Available online at www.sciencedirect.com

ScienceDirect

journal homepage: www.elsevier.com/locate/he

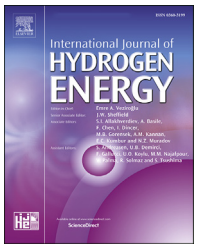

Understanding water-splitting thermochemical cycles based on nickel and cobalt ferrites for hydrogen production

Naiara B. Goikoetxea [a], *M. Belén Gómez-Mancebo* [a,*], *Rocío Fernández-Saavedra* [a], *Fernando Borlaf* [a], *Fernando García-Pérez* [a], *José Antonio Jiménez* [b], *Irene Llorente* [b], *Isabel Rucandio* [a], *Alberto J. Quejido* [a]

[a] *Chemistry Division, Research Centre for Energy, Environment and Technology (CIEMAT), Avda. Complutense 40, 28040 Madrid, Spain*

[b] *Department of Physical Metallurgy, National Center for Metallurgical Research (CENIM-CSIC), Avda. Gregorio del Amo 8, 28040, Madrid, Spain*

ARTICLE INFO

Article history:
Received 20 March 2019
Received in revised form
30 April 2019
Accepted 2 May 2019
Available online 31 May 2019

Keywords:
Water-splitting cycles
Hydrogen production
Mixed ferrites
Cyclability

ABSTRACT

Two step water-splitting cycles by using metal ferrites are considered as a clean and sustainable hydrogen production method, when concentrated solar energy is used to drive the thermochemical reactions. This process involves the reduction at very high temperature of the ferrite, followed by the water reoxidation to the original phase at moderate temperature, with the release of hydrogen. In order to decrease the temperature required to decompose the oxide, mixed ferrites of the type MFe_2O_4 with spinel crystal structure have been examined. In this sense, ferrites with the partial substitution of Co and Ni for Fe appear as successful materials in terms of hydrogen production and cyclability. In this work, commercial Ni and synthetic Co ferrites have been subjected to two water splitting cycles. The solid products obtained after thermal reduction and water decomposition reactions have been chemically and structurally characterized by WDXRF, XRD, XPS and SEM techniques, in order to get a deeper understanding of the mechanisms controlling the water splitting process. This knowledge contributes to improve the process involved in thermochemical cycles and to understand the lower efficiencies (H_2/O_2) for Co ferrite thermochemical cycles in comparison with those corresponding to Ni ferrite.

Introduction

As one of the most promising future energy carriers, hydrogen is currently produced from fossil resources using reforming or gasification processes, with the consequent release of carbon dioxide to the atmosphere. In fact, hydrogen can only be considered as an environmentally friendly and sustainable alternative to fossil energy carriers, if it is produced from renewable energy and without harmful emissions [1]. In that

* *Corresponding author.*
E-mail address: mariabelen.gomez@ciemat.es (M.B. Gómez-Mancebo).
https://doi.org/10.1016/j.ijhydene.2019.05.003

sense, the use of solar energy to produce hydrogen fulfils the requirements of a clean and renewable mechanism [2,3]. There are two main processes to obtain hydrogen using solar radiation. One is the water splitting by an electrolyser, driven by the electricity generated by a photovoltaic system. The other one is thermochemical water decomposition, in which water is decomposed into hydrogen and oxygen through intermediate reactions. This system, coupled with high temperature solar concentrators, offer higher solar to hydrogen system efficiency (up to 60–70%) compared to the conventional photovoltaic–electrolyser system because the intermediate process of solar energy conversion to electric power is eliminated [4]. Thermochemical cycles are composed by multi-step processes that form a closed cycle, in which the overall reaction is $H_2O \rightarrow H_2 + ½\ O_2$. Hydrogen and oxygen are produced in different steps and the intermediate reactants can be recycled [5–7].

Since Nakamura investigated the Fe_3O_4/FeO redox pair performance [8], many different redox pair systems have been reported in the literature [9–20]. In previous works, our group has evaluated the activity of several ferrites for hydrogen production by splitting water through thermochemical cycles [21–23], concluding that Ni and Co ferrites are the most promising ferrites for solar hydrogen production.

A two-step thermochemical cycle based on ferrites is divided in activation and hydrolysis step. In the activation step, a thermal reduction occurs, with the release of oxygen (Ec. 1). During the hydrolysis step, the ferrite is in contact with water from where it takes the oxygen to reduce, and hydrogen is released (Ec.2).

There are different reactions proposed in the literature [13,24]:

$$MFe_2O_4 \rightarrow (MO + 2\ FeO)_{ss} + \frac{1}{2}\ O_2 \qquad \text{Ec.1}$$

$$(MO + 2\ FeO)_{ss} + H_2O \rightarrow MFe_2O_4 + H_2 \qquad \text{Ec.2}$$

Where M = Ni, Co. But due to the formation of a reduced phase with a cell parameter similar to MO, another reaction could be possible in the activation step (Ec. 3).

$$3\ MFe_2O_4 \rightarrow 3\ MO + 2\ Fe_3O_4 + \frac{1}{2}\ O_2 \qquad \text{Ec.3}$$

A third reaction is also proposed in the activation step as a combination of the last two (Ec. 4):

$$2\ MFe_2O_4 \rightarrow (2\ MO + FeO)_{ss} + Fe_3O_4 + \frac{1}{2}\ O_2 \qquad \text{Ec.4}$$

Nevertheless, the specific reactions that take part in the process are still not well identified. In order to find out the reactions involved in the process and optimize the hydrogen production, an exhaustive chemical and structural characterization of the ferrites and reduced phases is needed. Thus, in this paper Ni and Co ferrites have been subjected to two water splitting cycles. A detailed chemical and structural characterization of the ferrites before and after the cycling assays has been carried out using WDXRF, XRD, XPS and SEM techniques, in order to achieve a deeper understanding of the activation step reaction mechanism and the whole thermochemical cycle process.

Experimental procedure

Synthesis

Commercial nickel ferrite nanopowder (<50 nm particle size) was supplied by Sigma-Aldrich and cobalt ferrite was synthetized by co-precipitation method using stoichiometric amounts of metal nitrates (Sigma-Aldrich) and NaOH as precipitation agent [22,23,25]. The precipitation was carried out under 90 min reflux, N_2 atmosphere and vigorous magnetic stirring. The co-precipitate was collected by centrifuging and washed with water and acetone. The final product was obtained by a thermal treatment at 1323 K, during 3 h and under Ar atmosphere [25]. In order to obtain $CoFe_2O_4$ powder sample, the as-prepared material was ground with an agate mortar.

Thermochemical cycles

Two-step thermochemical water splitting cycles were performed in a laboratory scale testing bench described elsewhere [21].

Powder samples were inserted into the electric furnace of the reaction system in a Pt/Rh crucible inside a mullite tube (20 mm outer and 17 mm inner diameters). Then, they were subjected to two thermochemical cycles. Essentially, activation step was performed at 1450 °C under Ar atmosphere for 4 h. For the hydrolysis step, temperature was reduced to 950 °C for 5 h under both Ar and steam atmosphere.

Characterization

During the thermochemical cycles, the outlet gas from the reaction chamber was forced to pass through a water trap. Then, the dry gas was introduced to a micro-gas chromatograph (Varian CP4900) to be analysed.

Chemical composition of the samples was determined by X-Ray fluorescence (XRF) (PANalytical, Axios) using a specific method developed for ferrites. The methodology was validated by contrasting the results with those obtained by Inductively Coupled Plasma Atomic Emission Spectroscopy (ICP-AES).

The morphology of the ferrites was observed by Scanning Electron Microscopy (SEM), using a Zeiss (Model EVO LS 15) microscope and semi-quantitative chemical micro-analysis was performed by an energy dispersive X-ray spectrometer (EDX) from Oxford (Model INCA-Energy 350).

X-Ray diffraction (XRD) studies with CuKα radiation were performed with a PANalytical X'Pert Pro diffractometer operating at 45 kV and 40 mA for determining the crystalline phases present in the samples. XRD data were collected in θ-θ configuration in the angular range of $20° < 2\theta < 80°$ with a 0.017° step size. Phase identification was obtained by the comparison method using the HighScore Plus software (PANalytical) and the Inorganic Crystal Structure Database (ICSD). Although XRD patterns obtained with Cu radiation can be used for simple phase identification purposes, this radiation may be not suitable for an accurate structural characterization and phase quantification. Due to the large

amount of Fe present in the samples, a relatively large part of Cu radiation will be absorbed. The intensity of the diffraction peaks will greatly reduce, making the measurement extremely long or impracticable to accumulate enough counts for a high degree of accuracy. For this reason, XRD measurements used for Rietveld refinements were carried out in a Bruker AXS D8 with Goebel mirror optic using a Co radiation generated at 40 kV and 30 mA. These scans covered 2θ values ranging from 15° to 125° with a step size of 0.01°.

Photoelectron (XPS) spectra were recorded using a Fisons MT500 spectrometer equipped with a non-monochromatic Mg Kα X-Ray source operated at 300 W and a hemispherical electron analyser (CLAM2) operating at constant pass energy of 20 eV which is typical of high-resolution conditions. The residual pressure in this ion-pumped analysis chamber was maintained below 10 8 torr during data acquisition. Specimen charging was corrected by setting the signal from adventitious C1s a 285.0 eV binding energy.

Results and discussion

In previous studies [15,26], it was observed that the amount of oxygen obtained during the first activation reaction is associated with a reaction mechanism involving oxygen release in several steps. Together with oxygen produced by activation step, oxygen absorbed by MFe_2O_4 during its synthesis is released when treating the sample to high temperature for the first time. For this reason, chemical and structural characterisation studies have been carried out during the first and second thermochemical cycles.

Original ferrites characterisation

Chemical composition of original $NiFe_2O_4$ (commercial ferrite) and $CoFe_2O_4$ (synthesised ferrite) determined experimentally by XRF is very similar to the stoichiometric composition, as shown in Table 1. Also it is possible to stand out that the amount of impurities in both ferrites do not exceed 1.0 wt %, as it was found in other ferrites characterised previously [21,26].

XRD patterns obtained for both ferrites show a single cubic spinel structure with a mean crystalline size of 11 and 98 nm, respectively, as calculated using the Scherrer equation. On the other hand, the measured lattice constants are in good agreement with those values reported in the Powder Diffraction File (PDF) cards of $NiFe_2O_4$ (PDF pattern 003–0875) and $CoFe_2O_4$ (PDF file 022–1086).

Thermochemical cycles characterization

Size and morphology of Ni and Co ferrite powders, and their evolution during the first two thermochemical cycles were characterized by SEM images. As shown in Figs. 1 and 2, all samples show the effect of sintering due to the high temperatures involved in the activation and hydrolysis reactions. Comparing both ferrites after the second activation step (Figs. 1a and 2a), it could be observed that Co ferrite shows bigger sized particles than Ni ferrite. Although morphology and grain size of Ni ferrite particles remain very similar after the second hydrolysis step (Fig. 1b), it is observed a decrease in the particle size for Co ferrite particles (Fig. 2b).

Semi-quantitative energy dispersive X-ray microanalyses were performed in a SEM-EDX for testing the homogeneity in chemical composition after the activation and hydrolysis reactions. Figs. 1 and 2 show elemental mappings for samples of Ni and Co ferrites after the second activation and hydrolysis steps, respectively. These figures show the segregation of Fe and Ni or Co during the activation reactions that was associated with the formation of a wustite phase characterized by a high content of Ni or Co, and then the remaining spinel phase would be enriched by Fe. These observations could indicate an activation reaction corresponding to Ec. 4. This segregation notably disappears in a significant way after the hydrolysis reaction, indicating that the spinel ferrite can be recovered during this reaction.

XRD patterns obtained, using Cu radiation, are displayed in Figs. 3 and 4 for Ni and Co ferrites, respectively. Fig. 3 shows that diffraction peaks of the starting spinel are sharpened by thermochemical cycles, due to the crystallite coarsening at the high temperatures used to drive the activation and hydrolysis reactions. This figure also shows new peaks corresponding to a wustite cubic structure after the first and second activation steps. Although the position of the diffraction peaks of this phase matches closely to the pattern of pure NiO (PDF pattern 003–0875), it can be observed a displacement of XRD lines toward pure FeO (PDF pattern 003–0875). This result was associated to the formation of a Ni rich solid solution of ($Ni_xFe_{1-x}O$) during the thermal reduction of Ni ferrite. After the hydrolysis step, this phase disappears and the original structure of the spinel ferrite is recovered. The appearance of a wustite phase during the activation steps of the thermochemical cycles was also observed in XRD patterns of Co ferrite samples, as shown in Fig. 4. This new phase corresponds to a solid solution $Co_xFe_{1-x}O$. Unlike in Co ferrite samples, a small amount of this phase can be observed in the XRD patterns after the hydrolysis steps, indicating that the oxidation process has not been completed.

Table 1 – Characterization data of the $NiFe_2O_4$ and $CoFe_2O_4$ ferrites.

FERRITE	Fe (%)[a]		Ni (%)[a]		Co (%)[a]		Lattice parameter a_o(Å)	Crystal size (nm) (Scherrer)[b]
	sto.	exp.	sto.	exp.	sto.	exp.		
$NiFe_2O_4$	47.7	48.0	25.0	26.0	–		8.32	11
$CoFe_2O_4$	47.6	45.3	–		25.1	23.3	8.37	98

[a] Wt%.
[b] Estimated by means of the Scherrer equation.

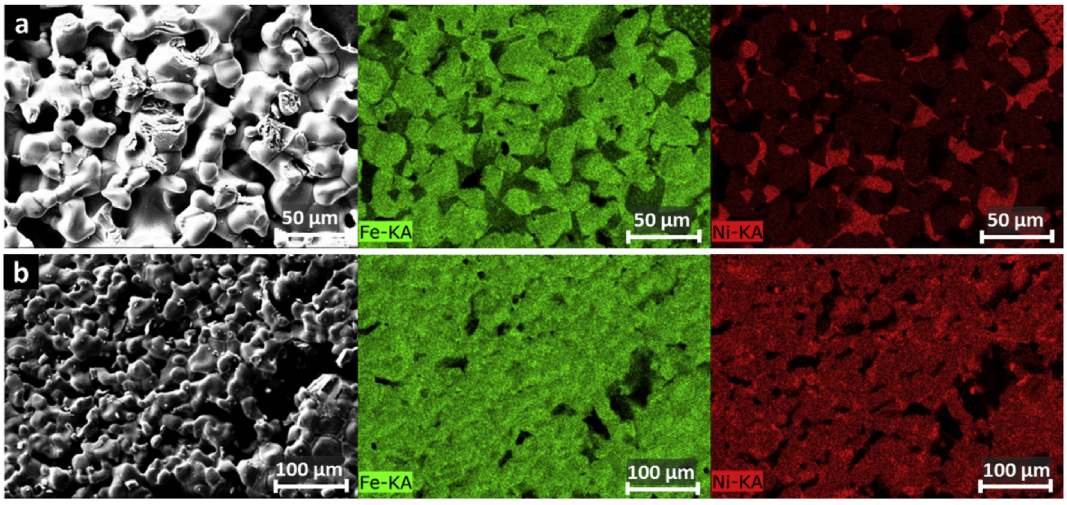

Fig. 1 – SEM photographs and mapping images of Ni ferrites after the second (a) activation step and (b) hydrolysis step.

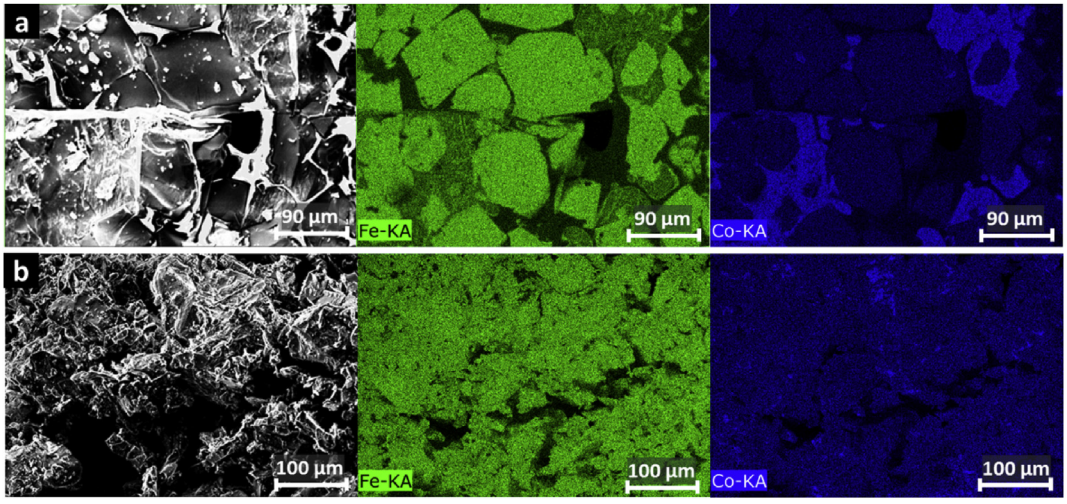

Fig. 2 – SEM images of sintered Co ferrites after the second (a) activation step and (b) hydrolysis step.

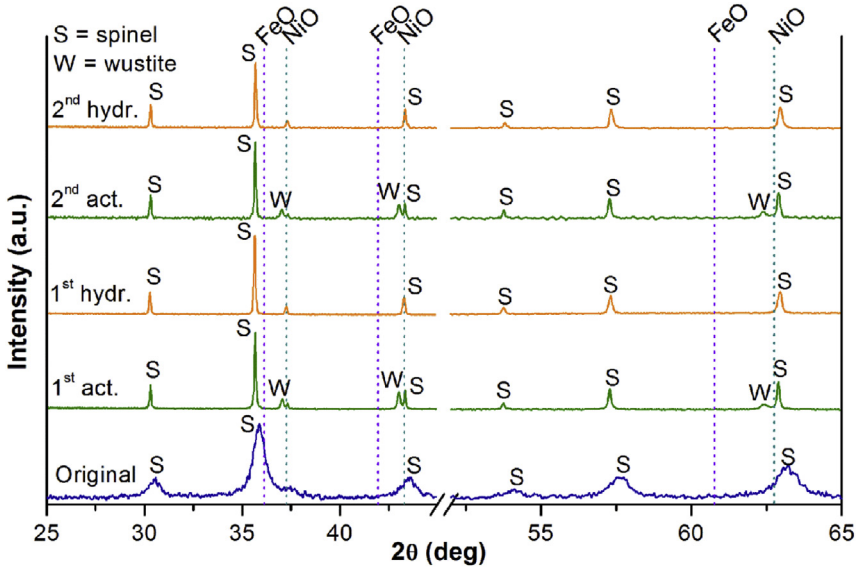

Fig. 3 – XRD patterns of Ni ferrites.

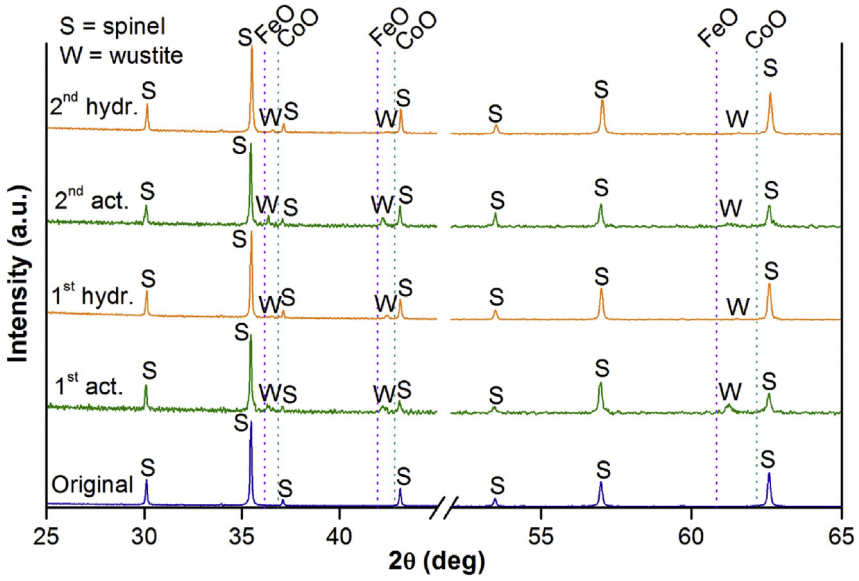

Fig. 4 – XRD patterns of Co ferrites.

Quantitative analyses of the crystalline phases identified from XRD patterns have been performed using the Rietveld method. We have used the version 4.2 of the TOPAS program (Bruker AXS) to model the full pattern with the crystallographic information of MFe_2O_4 spinel (M is Ni or Co) and a wustite like oxide, both obtained from Pearson's Crystal Structure databases (Pearson's Crystal Structure, Database for Inorganic Compounds, Release 2016/2017. Materials Park: ASM International, (2016)). In order to eliminate the instrumental broadening from the diffraction peaks of both phases, the instrument functions determined from the profile shape of an alumina plate standard measured under the same conditions. The figures of merit used to evaluate numerically the Rietveld refinement quality were: the weighted profile residual, R_{wp}, the statistically expected profile residual, R_{exp}, the profile residual factor, Rp, and the goodness of fit (sometimes referred as chi-squared), GoF [27]. Since GoF = R_{wp}/R_{exp}, a GoF = 1.0 means that the fit is as good as possible.

It has been shown that both Co and Ni readily can substitute Fe in MO binary oxides with the rock-salt structure due to the similarity in cation size of Fe^{2+}, Co^{2+} and Ni^{2+}, leading to the formation of solid solutions of $Ni_{1-X}Fe_XO$ and $Co_{1-X}Fe_XO$ (Table 2) [27]. Since the difference in lattice constant between NiO, FeO and CoO is lower that 3.5%, the local distortion in the lattice introduced by this cation substitutions makes that these mixed phases obey the Vegard's linear relation [28]. Thus, the value of the lattice constant deduced by the Rietveld refinement was used to calculate the composition parameter X of ternary oxides. As shown in Table 2, after the second activation cycle the Fe content in the wustite is higher in Co ferrite than in Ni ferrite. For this reason diffraction peaks of this phase are closer to pure FeO in Fig. 4 than in Fig. 3.

On the other hand the composition of the spinel was estimated considering the wustite stoichiometry together with bulk compositions determined by XRF and the percentage of spinel and wustite phases obtained by Rietveld refinement. Although estimated chemical composition of Ni and Co spinel phases after the second hydrolysis cycle, are close to perfect stoichiometry, the results reported in Table 2 show that the spinel phase in Co ferrites exhibits a more pronounced variation from the ideal value than Ni samples. The presence of a small amount of wustite causes a decrease on the Co content with respect to the theoretical stoichiometry. This observation confirms the results obtained by XRD using Cu radiation (Fig. 4) where the solid solution $Co_xFe_{1-x}O$ wustite phase is

Table 2 – Characterization data of Ni and Co ferrites after second activation and hydrolysis steps.

Ferrite	Step	Reaction Temp. (°C)	Spinel phase (%)[a]	Wustite phase (%)[a]	Bulk composition (%)[c]				Estimated spinel composition	Wustite composition[b]
					Ni	Co	Fe	O		
$NiFe_2O_4$	2 Act.	1450	71	29	25.55	–	45.33	27.23	$Ni_{0.11}Fe_{0.75}O_{1.31}$	$Ni_{0.84}Fe_{0.16}O$
	2 Hydr.	950	100	–	25.28	–	45.20	27.28	$Ni_{0.43}Fe_{0.81}O_{1,71}$	–
$CoFe_2O_4$	2 Act.	1450	84	16	–	20.04	45.91	29.88	$Co_{0.27}Fe_{0.67}O_{1.65}$	$Co_{0.30}Fe_{0.70}O$
	2 Hydr.	950	99	1.0	–	20.27	45.79	29.81	$Co_{0.34}Fe_{0.81}O_{1.85}$	$Co_{0.61}Fe_{0.39}O$

[a] Mass percentage estimated by Rietveld method.
[b] Estimated by Vegard's law.
[c] Mass percentage calculated by XRF. Results normalised to 100%.

identified in the XRD patterns after the hydrolysis steps, indicating that the oxidation process has not been completed.

The exhaustive XRD analysis performed to metal ferrites, with Cu and Co radiation, corroborates the results obtained by SEM-EDX where the spinel and wustite phases are identified and quantified in both, activation and hydrolysis steps.

XPS analysis has been used to distinguish the oxidation state of the cations present on the surfaces. For iron, two oxidation states could be expected in ferrites: Fe^{2+} at a binding energy of 709.7 and Fe^{3+} at 711.0 eV. In our samples, the binding energy of the $Fe2p_{3/2}$ obtained has been 710.7 and 710.9 eV for nickel ferrite (Fig. 5) and cobalt ferrite (Fig. 6), respectively, very close to the value of 711.0 eV reported for Fe_2O_3, confirming the predominance of Fe^{3+} on the ferrite surfaces.

Fig. 5 presents the XPS spectra of Fe 2p and Ni 2p in original $NiFe_2O_4$ and after first and second activation and hydrolysis steps. The 2p core photoelectron spectrum of the nickel ferrite, shows intense shake-up satellites at a higher binding

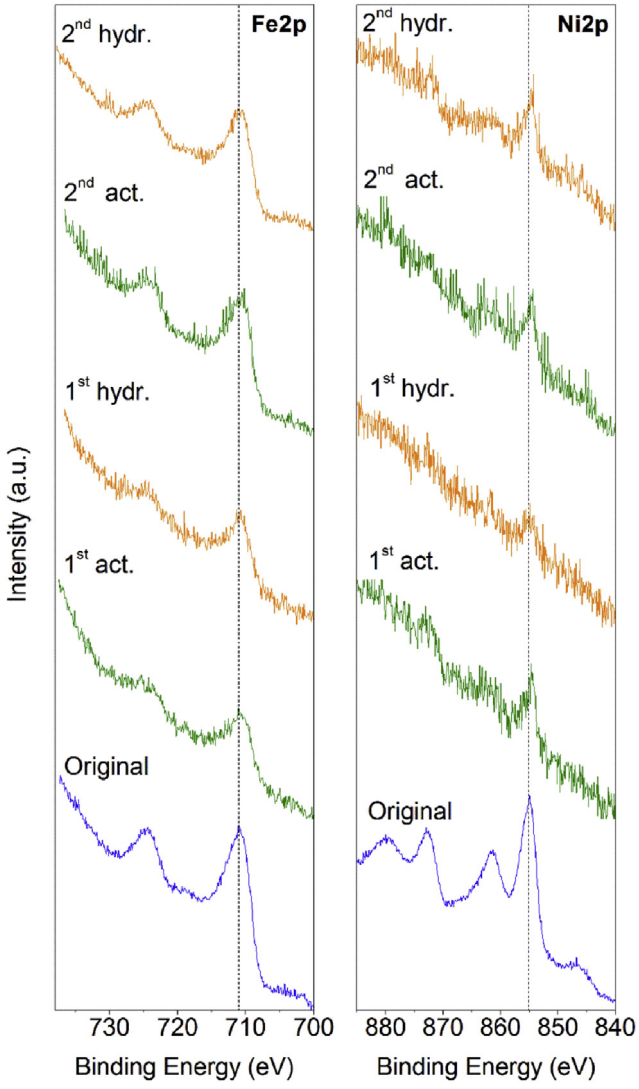

Fig. 5 – XPS spectra of Fe and Ni in original $NiFe_2O_4$ and after first activation step, first hydrolysis step, second activation step and second hydrolysis step.

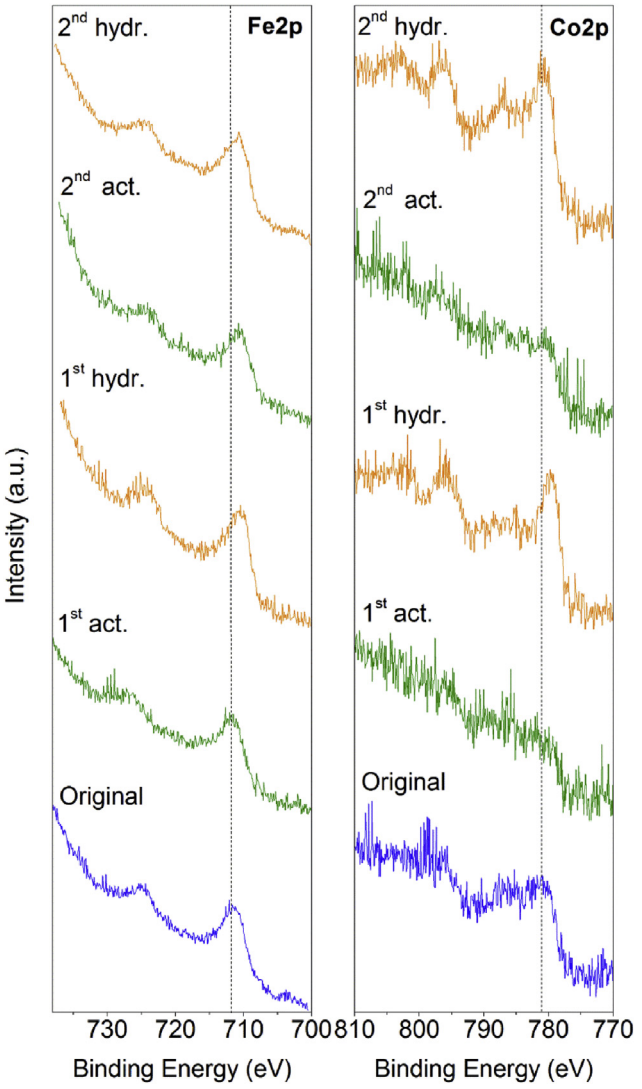

Fig. 6 – XPS spectra of Fe 2p and Co 2p in original $CoFe_2O_4$ and after first hydrolysis step, fist hydrolysis step, second activation step and second activation step.

energy (+6.3 eV) than the main photoelectron peak (854.4–855.0 eV), confirming the presence of only Ni^{2+} on the surface. As it can be observed, Fe spectra show a small shift to lower binding energy after activation steps. However, after hydrolysis steps Fe spectra are similar to the original one. Consequently, $NiFe_2O_4$ recovers its structure after thermochemical cycles.

Fig. 6 shows XPS spectra of Fe 2p and Co 2p in original $CoFe_2O_4$ and after first and second activation and hydrolysis steps. In this case, the spectra of Fe after hydrolysis steps show a permanent shift to lower binding energy, and then it is reasonable to think that $CoFe_2O_4$ cannot recover its structure completely after thermochemical cycles.

Water splitting cycles

Co and Ni ferrites are subjected to two thermochemical cycles assays in a laboratory scale testing bench. The amounts of oxygen and hydrogen per gram of ferrite released during

Table 3 – Gases evolution and hydrolysis reaction yield during two consecutives thermochemical cycles.

Ferrites	Cycle	mmol O_2/g	mmol H_2/g	H_2/O_2
$NiFe_2O_4$	1°	0.52	0.58	1.12
	2°	0.46	0.50	1.09
$CoFe_2O_4$	1°	0.58	0.83	1.43
	2°	0.52	0.85	1.63

activation and hydrolysis steps, respectively, are estimated from the numerical integration of the molar flow vs. time curves obtained in each step of the cycle. These results together with the ratio between them, which indicates the hydrolysis reaction yield, are summarized in Table 3.

Both $NiFe_2O_4$ and $CoFe_2O_4$ ferrites present a higher amount of oxygen released for the first cycle, owing to processes related to the presence of oxygen absorbed on the sample surfaces during their synthesis, which is released when treating the samples to high temperature only during this first cycle. Comparing both materials, synthesised $CoFe_2O_4$ is able to produce a larger amount of hydrogen per cycle than commercial Ni ferrite.

The experimental H_2/O_2 ratio (Table 3) has been considered as an indicator for potential cyclability, since a production of hydrogen closer to the stoichiometric amount (the stoichiometric ratio for the water splitting reaction is 2) means a higher recovery of the original ferrite from the partially reduced sample, which should lead to a higher activity towards the next cycle. After two thermochemical cycles, $CoFe_2O_4$ shows better recovery than $NiFe_2O_4$ since the H_2/O_2 ratio is closer to the stoichiometric ratio. This behaviour partially disagrees with XRD results, where peaks ascribed to wustite phase are observed after the second hydrolysis step. However, Rietveld refinement estimates that mass percentage of wustite phase is as low as 1% (Table 2). In addition, in previous studies carried out in our group, where the cyclability of both ferrites was evaluated [29], it was concluded that Ni powder samples shown the best behaviour in terms of hydrogen production after ten cycles, because the amount of wustite phase in Co ferrite increased after each cycle.

Conclusions

Commercial Ni and synthetic Co ferrites have been subjected to two water splitting cycles. The solid products obtained after each step of the two cycles have been chemically and structurally characterized by different techniques in order to get a deeper understanding of the reaction mechanism of this process.

XRD (including Rietveld analysis), XPS and elemental mappings of Ni and Co show beside the spinel phase corresponding to the original ferrite, the presence of a new wustite phase of the type, $Me_{1-x}Fe_xO$ (where Me = Ni or Co) after the second activation step due to the partial reduction of the spinel ferrites. After the hydrolysis step, a homogeneous distribution through the sample of Fe and Ni or Co is observed. However, the total recovery of the original spinel ferrite is only demonstrated for Ni ferrite. Considering all these results, it could be deduced that the third reaction mechanism proposed for the activation step (Ec. 4) would be the most appropriate to describe the process that takes place in the thermochemical cycles for Co and Ni ferrites, where a sintered solid solution of the type $Me_{1-x}Fe_xO$, where Me = Ni or Co, would be formed.

Evaluation of the ability of Ni and Co ferrites for producing hydrogen by water splitting during two thermochemical cycles determines that Co ferrite is able to produce a higher amount of hydrogen than Ni ferrite. In addition, H_2/O_2 ratio during these two cycles is higher for Co ferrites. However as it was previously reported, it was proved that after ten cycles the efficiency of Co ferrites is lower than Ni ferrites because of the enrichment of Co ferrites in wustite phase, which in turn implies the uncomplete recovery of the spinel phase throughout the cycles, as it was deduced from XRD and XPS results.

This exhaustive study of each step of Ni and Co ferrite thermochemical cycles for hydrogen production has provided a better understanding of the reaction mechanism involved in these cycles. This knowledge contributes to improve the process involved in thermochemical cycles and thus be able to increase the total amount of oxygen and hydrogen generated.

In addition, this in-depth study has contributed to understand the lower efficiencies (H_2/O_2) for Co ferrite thermochemical cycles in comparison to those corresponding to Ni ferrite after 10 consecutive cycles.

Acknowledgments

European Regional Development Fund is gratefully acknowledged by the partial funding of the XRF and XRD equipment employed for this study (Projects FEDER 2004 CIEM05-34-030 and FEDER 2004 CIEM05-34-031).

REFERENCES

[1] Graf D, Monnerie N, Roeb M, Schmitz M, Sattler C. Economic comparison of solar hydrogen generation by means of thermochemical cycles and electrolysis. Int J Hydrogen Energy 2008;33:4511–9.
[2] Carrillo RJ, Scheffe JR. Advances and trends in redox materials for solar thermochemical fuel production. Sol Energy 2017;156:3–20.
[3] Bhosale RR. Thermodynamic analysis of Ni-ferrite based solar thermochemical H2O splitting cycle for H2 production. Int J Hydrogen Energy 2019;44:61–71.
[4] Hosseini SE, Wahid MA. Hydrogen production from renewable and sustainable energy resources: promising green energy carrier for clean development. Renew Sustain Energy Rev 2016;57:850–66.
[5] Kodama T, Gokon N. Thermochemical cycles for high-temperature solar hydrogen production. Chem Rev 2007;107:4048–77.
[6] Steinfeld A, Meier A. Solar fuels and materials. Encyclopedia of Energy 2004;5:623–37.
[7] Gobara HM, Nassar IM, El Naggar AMA, Eshaq G. Nanocrystalline spinel ferrite for an enriched production of hydrogen through a solar energy stimulated water splitting process. Energy 2017;118:1234–42.

[8] Nakamura T. Hydrogen production from water utilizing solar heat at high-temperatures. Sol Energy 1977;19:467–75.
[9] Agrafiotis C, Roeb M, Konstandopoulos AG, Nalbandian L, Zaspalis VT, Sattler C, et al. Solar water splitting for hydrogen production with monolithic reactors. Sol Energy 2005;79:409–21.
[10] Han SB, Kang TB, Joo OS, Jung KD. Water splitting for hydrogen production with ferrites. Sol Energy 2007;81:623–8.
[11] Kaneko H, Gokon N, Hasegawa N, Tamaura Y. Solar thermochemical process for hydrogen production using ferrites. Energy 2005;30:2171–8.
[12] Kaneko H, Kojima N, Hasegawa N, Inoue M, Uehara R, Gokon N, et al. Reaction mechanism of H_2 generation for $H_2O/Zn/Fe_3O_4$ system. Int J Hydrogen Energy 2002;27:1023–8.
[13] Kodama T, Gokon N, Yamamoto R. Thermochemical two-step water splitting by ZrO_2-supported $Ni_xFe_{3-x}O_4$ for solar hydrogen production. Sol Energy 2008;82:73–9.
[14] Miller JE, Allendorf MD, Diver RB, Evans LR, Siegel NP, Stuecker JN. Metal oxide composites and structures for ultra-high temperature solar thermochemical cycles. J Mater Sci 2008;43:4714–28.
[15] Agrafiotis C, Pagkoura C, Zygogianni A, Karagiannakis G, Kostoglou MG, Konstandopoulos A. Hydrogen production via solar-aided water splitting thermochemical cycles: combustion synthesis and preliminary evaluation of spinel redox-pair materials. Int J Hydrogen Energy 2012;37:8964–80.
[16] Roberts SJ, Dodson JJ, Carpinone PL, Hagelin-Weaver HE. Evaluation of nanoparticle zirconia supports in the thermochemical water splitting cycle over iron oxides. Int J Hydrogen Energy 2015;40:15972–84.
[17] Fresno F, Yoshida T, Gokon N, Fernández-Saavedra R, Kodama T. Comparative study of the activity of nickel ferrites for solar hydrogen production by two-step thermochemical cycles. Int J Hydrogen Energy 2010;35:8503–10.
[18] Muroyama AP, Schrader AJ, Loutzenhiser PG. Solar electricity via an Air Brayton cycle with an integrated two-step thermochemical cycle for heat storage based on Co3O4/CoO redox reactions II: kinetic analyses. Sol Energy 2015;122:409–18.
[19] Alvani C, Ennas G, La Barbera A, Marongiu G, Padella F, Varsano F. Synthesis and characterization of nanocrystalline $MnFe_2O_4$: advances in thermochemical water splitting. Int J Hydrogen Energy 2005;30:1407–11.
[20] Lorentzou S, Pagkoura C, Zygogianni A, Karagiannakis G, Konstandopoulos AG. Thermochemical cycles over redox structured reactors. Int J Hydrogen Energy 2017;42:19664–82.
[21] Fresno F, Fernández-Saavedra R, Gómez-Mancebo MB, Vidal A, Sánchez M, Rucandio MI, et al. Solar hydrogen production by two-step thermochemical cycles: evaluation of the activity of commercial ferrites. Int J Hydrogen Energy 2009;34:2918–24.
[22] Fernández-Saavedra R, Sánchez M, Vidal A, Gómez-Mancebo MB, Gómez-López LV, Rucandio MI, et al. Synthetic ferrites for solar hydrogen production through two-step thermochemical cycles. III iberian symposium on hydrogen. Fuel Cells and Advanced Batteries Zaragoza 2011:109–12.
[23] Fernández-Saavedra R, Fresno F, Sánchez M, Vidal A, Gómez-Mancebo MB, Gómez-López LV, et al. Hydrogen production by two-step water splitting themochemical cycles using mixed iron oxides. Hypothesis IX 2011. San José (Costa Rica).
[24] Gokon ST, Yamamotoa H, Kodamaa T. Thermochemical two-step water-splitting reactor with internally circulating fluidized bed for thermal reduction of ferrite particles. Int J Hydrogen Energy 2008;33:2189–99.
[25] Kodama T, Wada Y, Yamamoto T, Tsuji M, Tamaura Y. Synthesis and characterization of ultrafine nickel (II)-bearing ferrites ($Ni_xFe_{3-x}O_4$, x=0.14-1.0). J Mater Chem 1995;5:1413–8.
[26] Fernández-Saavedra R, Gómez-Mancebo MB, Caravaca C, Sánchez M, Quejido AJ, Vidal A. Hydrogen production by two-step thermochemical cycles based on commercial nickel ferrite: kinetic and structural study. Int J Hydrogen Energy 2014;39:6819–26.
[27] Schmidt P. How to get ternary solid solutions Fe1–xM′xO (M = Co, Ni)? A thermodynamic concept. Eur J Inorg Chem 2008;2008:2847–55.
[28] Vegard L. The constitution of the mixed crystals and the filling of space of the atoms. Zeitschrift Fur Physik 1921;5:17–26.
[29] Goikoetxea NB, Gómez-Mancebo MB, Fernández-Saavedra R, García-Pérez F, Jiménez JA, Rodríguez J, et al. Study of the performance of Co and Ni ferrites after several cycles involved in water-splitting thermochemical cycles. Int J Hydrogen Energy 2016;41:16696–704.